RESEARCH ARTICLE OPEN ACCESS

Wavelet-Based Fault Location and Distance Protection Method for Transmission Lines

K. Prasanna Kumar[1], K. Durga Syam Prasad[2], K. Sravanthi[3]
[1] P.G Student, Department of EEE, DIET College Of Engineering, Visakhapatnam- 531 002
[2] Sr. Assistant Professor, Department of EEE, DIET College Of Engineering, Visakhapatnam- 531 002
[3]Assistant Professor, Department of EEE, Vignan's Institute of Information Technology, Visakhapatnam.

Abstract
This paper presents a single-ended traveling wave -based fault location and distance protection method for a hybrid transmission line: an overhead line combined with an underground cable. Dis-crete wavelet transformation (DWT) is used to extract transient information from the measured voltages. Support vector machine (SVM) classifiers are utilized to identify the faulty-section and faulty-half. Bewley diagrams are observed for the traveling wave patterns and the wavelet coeffi cients of the aerial mode voltage are used to locate the fault. The transient simulation for different fault types and locations are obtained by ATP using frequency - de-pendent line and cable models. MATLAB is used to process the simulated transients and apply the proposed method. The perfor-mance of the method is tested for different fault inception angles (FIA), different fault resistances, non-linear high impedance faults (NLHIF), and non-ideal faults with satisfactory results. The impact of cable aging on the proposed method accuracy is also investigated.
Index Terms—Alternative transients program (ATP), fault lo-cation, frequency -dependent line model, support vector machine, travelling waves, underground cable, wavelet transformation.

I. INTRODUCTION

A. Motivation and Literature Review

In Tomorrow's Smart grid, fast and accurate fault lo-cation along power transmission and distribution networks will be achieved by deployment of modern technologies used for data recording and analysis combined with intelligent al-gorithms. Smart fault location will result in power system re-liability improvement, quick restoration of the power service and reduction in outage time [1]. The proliferation of under-ground cables combined with overhead transmission lines (hy-brid transmission) in medium- and high -voltage will increase in the future grid. "Hybrid transmission" systems are preferred when right-of-way related issues arise and they offer better reli-ability. In addition, underground cables are also used to connect off-shore wind farms to the existing grid through overhead lines. However, the complexity of fault location problem increases with the proliferation of such an unusual topology.

The fault location methods for overhead lines or underground cables are based on post-fault phasors; traveling waves or artifi-cial intelligence. Traveling wave-based fault locators are more accurate, and more reliable when compared to phasor-based methods; however they require advanced sensors with high sampling rates.

Future grid can employ traveling wave- based methods by taking advantage of modern technologies such as optical transducers instead of conventional CTs and CVTs. The main challenge in traveling wave-based fault location for combined overhead line and underground cable is faulty-sec-tion identification. This challenge is due to the reflections of the fault signal from the joint-node and the fault point as well as the unequal traveling wave velocities in line and cable. This paper uses support vector machine (SVM) and discrete wavelet transformation (DWT) to address these challenges and proposes a new traveling wave-based fault location method. Following is an overview of the use of DWT and SVM in power system fault location followed by the review of fault location methods for cable.

The use of SVM for faulty- section identification in series com-pensated transmission line is proposed in [2]–[4]. In [2] steady-state post-fault voltages and currents are used as the input to the SVM classifier, while the current transients are the inputs to the SVM faulty-section identifier in [3] and voltage transients are utilized as the input to the SVM in [4]. The proposed methods in [3] and [4] are dependent on the fault type. In [5] fault lo-cation in transmission lines using SVM- Neural Network with voltage and current transients is proposed. The proposed method assumes that the fault type is known and the SVM corresponding to the fault type is used. References [6] and [7] propose a fault classifi cation and location method based on wavelet transform, SVM, and ANN. The wavelet transformation coeffi cients of three- phase voltage and current transients are used as the input to the SVM fault classi fiers. The ANN is

then used for fault lo-cation according to the identified fault type.

The single-ended fault location in underground cable using steady -state post-fault phasor voltage and current measure-ments are proposed in [8] and [9]. The faulted underground cable is modeled using the distributed line model. Offline traveling wave-based fault location methods for underground cables are proposed in [10] and [11] where the traveling waves are generated by applying an external excitation voltage. A real -time single- ended traveling wave -based fault location for underground cable is proposed and implemented in [12]. Voltage and current transients are recorded by 200-MHz optic measurements. In [13] a two-ended traveling wave-based fault location using current transients recorded by optic CTs is implemented. The use of discrete wavelet transform (DWT) for transmission line fault location is first proposed in [14]. DWT is applied to the aerial mode voltage to extract the traveling wave information from the recorded transients. In [15] and [16], two -ended traveling wave-based fault locations are pro-posed for underground cables. The time delay between arrivals of traveling waves at both ends is used to calculate the fault location. In [17] and [18] phasor-based fault location methods for hybrid transmission line consisting of an overhead line an underground cable are proposed.an underground cable are proposed. The proposed methods uti-lize the synchronized voltage and current measurements from both ends of the transmission line. In [19] an adaptive neural network-fuzzy approach is used to locate the fault accurately in a combined transmission line using fundamental compo-nents of post-fault measured voltages. In [20] a single-ended traveling wave - based fault-location method using discrete and continuous wavelet transformation is implemented. The current transients are recorded by using 1.25 MHz optical current transducers. [21] presents a wavelet-fuzzy fault location method for transmission lines. DWT is applied to the current transients and the current wavelet energies are used as the input to the fuzzy fault location algorithm. In [22], a two-ended fault location method using the DWT coefficients at 97–195 Hz fre-quency band of three-phase current transients is proposed. The algorithm is dependent on fault type. Cubical interpolation is finally utilized to determine the exact fault location. Reference [23] presents a wavelet and neuro -fuzzy based fault location method. Voltage and current DWT coefficients are used as the input for faulty-section identification. The impedance-based fault location method is then utilized which is dependent on fault type. In [24], a single-ended traveling wave-based fault location method for combined transmission lines is proposed. The voltage traveling wave's polarity change is used to identify the faulty-section. The time delay between traveling waves is then used to calculate fault location. References [25] and [26] present traveling wave-based fault location methods for underground cables using DWT. [25] uses DWT to cancel the noise and detect the arrival instant of waves observing the correlation between wavelet scales. [26] assumes that the mea-surements are synchronized at both ends. In [27], a combined wavelet-neural network based fault classification and location is proposed. The authors use scale- 3 wavelet coefficients of voltages and fast Fourier transform of reconstructed voltage signal at the same scale to train the neural network.

B. Contribution and Paper Organization

This paper presents a single-ended fault location method based on traveling waves for a hybrid transmission line, which is composed of an overhead line combined with an underground cable. The preliminary results are presented in [28] and this paper extends the analyses. The method uses DWT and SVM for faulty -section/half identification. The main contributions of the paper are as follows:

- The proposed method uses SVM for faulty-section identi-fication, which is independent of fault type.
- The faulty-half identification is improved by utilization of SVM instead of the time-delay between the arrival time of the initial travelling waves in ground mode and aerial mode.
- The SVM classifiers use a smaller set of inputs for decision making.

The SVM identifiers use the normalized voltage wavelet ener-gies and the normalized transient current energies as input. The performance of the proposed method is insensitive to the fault in-ception angle (FIA) and the method is tested for different fault resistances, non-linear high impedance faults (NLHIF) and non-ideal faults. The impact of cable aging on the proposed fault loca-tion method is also discussed. This paper is organized as follows: In Section II, the fundamentals of SVM classifiers are brie fly re-viewed. In Section III, the proposed fault location method based

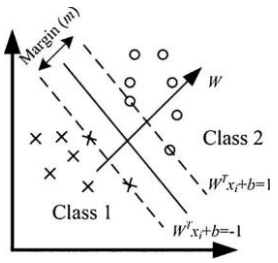

Fig. 1. 2-dimensional feature space with the optimal separating hyperplane [30].

on DWT and SVM is presented. Simulation results are provided in Section IV followed by the conclusions in Section V.

II. REVIEW OF SUPPORT VECTOR MACHINES (SVM)

Support vector machine (SVM) was first introduced by Vapnik as a binary linear classifier [29]. The SVM classi fica-tion finds an optimal hyperplane to separate data sets with two different classes({+1,-1}). The linear hyperplane is defined by a weight vector W and a bias term b as:

$$W^T x + b = \begin{cases} \geq 1, \text{class} + 1 \\ \leq -1, \text{class} - 1 \end{cases} \quad (1)$$

Fig. 1 shows the separating hyperplane in a 2-dimensional space. The separation margin (m) between two classes is given as [30]:

$$m = \frac{2}{\|w\|} \quad (2)$$

In order to maximize m, $\|W\|$ is minimized.thus the maximum margin ,m can be found by solving the following quadratic optimizing problem [30]:

$$\min \frac{1}{2}\|w\|^2 \quad (3)$$

subject to $y_i(W^T x_i + b) \geq 1$ (4)

Where $y_i \in \{-1,+1\}$ is the corresponding label for each x_i.

The solution to the problem provides the values of w and b such that the separation between the classes is maximum. The SVMs are obtained by solving the following dual optimization problem [30]:

$$\max L(\alpha) = \sum_{i=1}^{N} \alpha_i - 2^{-1} \sum_{i=1}^{N} \sum_{i=1}^{N} \alpha_i \alpha_j y_i y_j x_i x_j \quad (5)$$

Subject to $\sum_{i=1}^{N} \alpha_i y_i$ (6)

$$\alpha_i \geq 0 \quad (7)$$

where αi is the Lagrangian multiplier and N is the number of training data.

Once the dual optimization problem is solved, the training points with $\alpha_i > 0$ are the support vectors (SVs), and then W_* and b_* are calculated as [30]

$$w^* = \sum_{i=1}^{N_{SV}} \alpha_i^* y_i x_i \quad (8)$$

$$b^* = \frac{1}{N_{sv}} \left(\sum_{i=1}^{N_{SV}} y_i - w^* x_i \right) \quad (9)$$

where N_{SV} is the number of SVs.

However, if the original data in the input space is not linearly separable, it can be mapped into a higher dimensional feature space using non-linear functions Φ to obtain a linearly separable data set. As calculation of inner product of Φ in higher dimen-sional feature space is computationally complex, kernel func-tion k; is utilized to calculate the inner product directly as a func-tion of the original data in the input space. Thus, the SVMs are obtained by solving the following optimization problem [30]:

$$\max L(\alpha) = \sum_{i-1}^{N} \alpha_i - 2^{-1} \times \sum_{i-1}^{N} \sum_{j-1}^{N} \alpha_i \alpha_j y_i y_j k(x_i, x_j) \quad (10)$$

$$\text{subject to } \sum_{i-1}^{N} \alpha_i y_i = 0 \quad (11)$$

where $k(x_i, x_j)$ is the kernel function.

Thus, the optimization problem is solved and the training points with $\alpha_i > 0$ are the SVs. The optimal decision function is then expressed as follows [30]:

$$\text{sign}\left(\sum_{i \in SV} \alpha_i^* y_i \cdot k(x, x_i) + b^* \right) = \begin{cases} > 0 & \text{class} + 1 \\ < 0, & \text{class} - 1 \end{cases} \quad (12)$$

$$b^* = \frac{1}{N_{SV}} \left(\sum_{i=1}^{N_{SV}} y_i \sum_{j=1}^{N_{SV}} \alpha_j^* y_j k(x_i, x_j) \right) \quad (13)$$

The most commonly used kernel functions such as linear, sig-moidal, and Gaussian radial basis function (RBF) are tested for training and evaluating the SVM classifiers in this paper and the Gaussian RBF is chosen due to its better performance. The Gaussian RBF kernel function is given as:

$$K(x_i,x_j) = \exp(-(\|x_i - x_j\|^2)/\gamma \quad (14)$$

Where x_i and x_j are n-dimensional input vectors . $\gamma = 2\sigma^2$,

σ is the standard deviation of the Gaussian. The kernel function parameter (γ) is tuned only once in order to achieve sufficient accuracy. For a more detailed review of SVM, refer to [30].

In the following section, the proposed fault location method based on SVM and DWT are presented.

III. PROPOSED METHOD FOR FAULT LOCATION

This section describes the proposed single-ended traveling wave-based fault location method for a hybrid transmission line including an overhead line combined with an underground cable. The one-line diagram of the transmission line is shown in Fig. 2, where L_L is the length of the overhead line, L_C is the length of the underground cable and M is the

measurement location.

The fault location is developed based on the following as-sumptions:

Measurements at the sending end of overhead line are available.

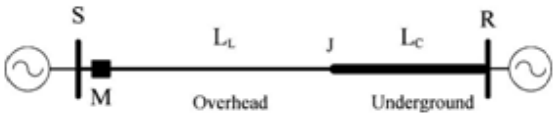

Fig. 2. A 230-kV transmission line including an overhead line combined with an underground cable.

- The measurements are obtained through optic voltage and current recorders instead of conventional CVTs and CTs.
- Measurement devices are not available at the joint point.
- Generation and load are not present at the joint point. The proposed fault location method is summarized as fol-lows:

A. The faulty-section (i.e., line or cable) is identified using a binary SVM classier.
B. The faulty-half is identified by using another binary SVM corresponding to the faulty-section.
C. The Bewley diagram of the fault-initiated travelling waves is used for fault location.

Note that each topology (different tower con figuration, dif-ferent phase configuration, different conductor, different line/ cable length, etc.) requires a different training of support vector machines. The three steps outlined above are described in the following subsections.

A. SVM Faulty-Section Identification

Faulty-section identification is performed using a binary sup-port vector machine, SVM1 . The SVM1 output implies whether the fault is in the overhead line (+1) or in the underground cable (_1) . The SVM1 classifier needs to be trained using different fault scenarios in a given topology. The performance of the SVM1 classifier is then evaluated using other fault scenarios.

The magnitude of voltage and current transients change with respect to fault location, fault inception angle (FIA) and fault re-sistances subsequently affecting the calculated voltage wavelet energies and current energies. In this paper, normalized wavelet energies of three-phase and ground mode transient voltages and normalized energies of three- phase and ground mode transients currents are used as input to the binary SVM classifiers. Nor-malization prevents having large weight vectors (W_*) in (8) and over-fitting for the SVMs. The classification is tested using three different wavelets: Daubechies- 4 (db-4), db-8, and Meyer. The classification accuracy for three wavelets remains the same and db-4 is utilized as the mother wavelet in this paper. The input feature extraction steps for the SVM classifiers are provided as follows:

1. Clarke's modal transformation for transposed lines is ap-plied to three-phase voltages to obtain aerial and ground mode voltages. In the case of untransposed lines, the modal transformation matrix obtained by ATP software can be used.
2. DWT is applied to three phase voltages($v_{a,}v_{b,}v_{c}$) and ground-mode voltage(V_0) to obtain the wavelet transfor-mation coefficients (WTCs) in scale -2. The selection of scale-2 over scale-1 is due to better performance for the investigated circuits in this study. WTCs are then squared to identify the arrival instants and hereafter denoted WTC2 s

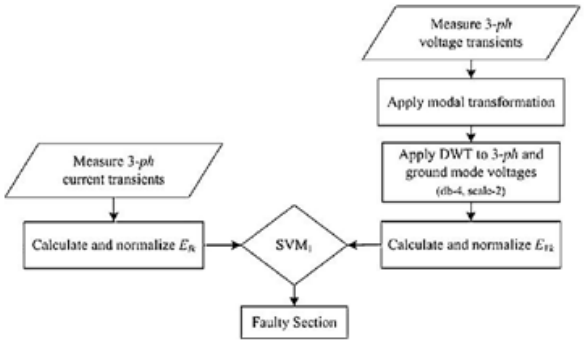

Fig. 3. Faulty-section identification flowchart.

3. The energies of voltage wavelet coeffi cients, Evk and cur-rents, $Eik(k\in\{abcand0\})$ are calculated over one cycle after the fault is detected as follows:

$$E_{Vk} = \sum_{m=0}^{M-1} \mathrm{WTC}_k^2(m) \text{ for } k \in \{a, b, c \text{ and } 0\} \quad (15)$$

$$E_{Ik} = \sum_{m=0}^{M-1} I_k^2(m) \text{ for } k \in \{a, b, c \text{ and } 0\} \quad (16)$$

where Evk is the voltage wavelet energy, Eik is the current energy and M is the number of samples in one cycle.

4. The voltage wavelet energies and current energies are nor-malized as:

$$E_{Nvk} = \frac{E_{Vk}}{E_{Va} + E_{Vb} + E_{Vc} + E_{V0}} \quad (17)$$

Where k∈{a,b,c,0}

$$E_{Nvk} = \frac{E_{Ik}}{E_{Ia} + E_{Ib} + E_{Ic} + E_{I0}} \quad (18)$$

Where k∈{a,b,c,0}

Where E_{Nvk} is the normalized voltage wavelet energy and

$E_{N_{1k}}$ is the normalized current energy.

The training is carried out to obtain the optimum decision function for the binary SVM.The input features,E_{Nvk} and E_{Nik} are stored in an N× 8 matrix where each column represents one feature and each row represents one training sample. N is the total number of different fault scenarios with different locations, types, FIAs, loadings, and fault resistances. The flowchart of the algorithm is provided in Fig. 3. SVM1 is trained using the training matrix corresponding to an 8-dimen-sional feature space. Once the training process is completed and the optimal decision function for the two-class separation is known, the SVM1 is ready to identify the faulty-section.

B. SVM Faulty-Half Identification

The existing traveling wave-based fault location methods use the time delay between the arrival time of the initial travelling waves in ground mode and aerial mode for faulty-half identifi-cation. In this paper, SVM is utilized for faulty -half identifi ca-tion, which makes the algorithm insensitive to the possible er-rors resulting from calculation of the time delay, especially for the faults close to the middle of the lines. The faulty-half SVM identifiers are trained by using E_{Nvk} and E_{Nik} described in the

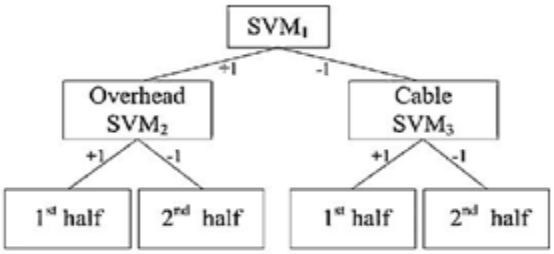

Fig. 4. Faulty-half identification DT-SVM diagram.

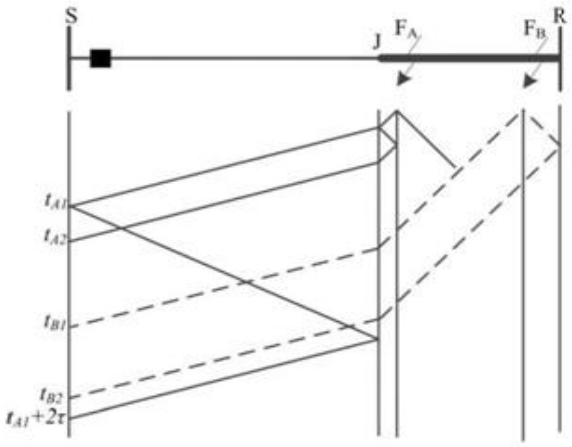

Fig. 5. Bewley diagram of faults in underground cable.

previous section. The SVM based decision tree (DT-SVM) for faulty-half identification is shown in Fig. 4, where SVM2 and SVM3 are utilized for faulty-half identification in the overhead line and underground cable, respectively. Using a trained SVM for each section (i.e., line or cable) for all fault types is another advantage of the proposed method.

C. Fault Location

Once the faulty-section and half are identified, the single-ended traveling wave-based is utilized for fault location. For the faults located in the underground cable (F_A and F_B in Fig. 5), the first peak of the traveling wave arrives at bus S at time t_{A1} . The first reflected backward travelling wave from the joint point arrives at bus S after t_{A1} with a time delay, 2τ where τ is the time required for a traveling wave to travel the full length of the line. Since the overhead line travelling wave velocity (ν_{line}) and the line length (L_L) are known, 2τ can be calculated as:

$$2\tau = \frac{2L_L}{\nu^{\text{line}}} \tag{19}$$

The travelling waves arriving at time instants $n\tau(n=2,4,6,\ldots)$ after the fi rst observed traveling wave are *not* used for fault location. For a fault in the fi rst half of the cable, the fault location from bus S is calculated by using:

$$x = L_L + \frac{\nu^{\text{cable}} \cdot \blacktriangle t}{2} \tag{20}$$

where ν_{cable} is the propagation velocity along the underground cable calculated at the frequency corresponding to the middle value of scale -2 and Δt [s] is the time delay between the first (t_{A1}) and the second peak (t_{A2}) aerial mode voltage WTC2 s in scale-2 at bus S corresponding to backward traveling wave and the reflected backward traveling wave from the fault point, respectively. For a fault in the second half of the underground cable, the fault location is calculated by using:

$$x = L_L + L_C - \frac{\nu^{\text{cable}} \cdot \blacktriangle t}{2} \tag{21}$$

where L_C [mi] is the length of the underground cable and Δt [s] is the time difference between the first (t_{B1}) and the second peak (t_{B2}) of WTC2 s at bus S corresponding to the backward traveling wave and the reflected forward traveling wave from bus R, respectively.

The single-ended traveling wave-based method developed in [14] is utilized to locate the faults identified by SVMs in over-head line. For a fault in the first half of the overhead line, the time delay between the first and the second traveling waves, Δt [s] is used to calculate the fault location. The time delay is de-termined by observing aerial mode voltage WTC2 s in scale-2. Fault location is calculated as:

$$x = \frac{\nu^{\text{line}} \cdot \blacktriangle t}{2} \tag{22}$$

where ν_{line} [mi/s] is the propagation velocity in the

overhead line calculated at the frequency corresponding to the middle value of scale-2. For the faults identified in the second half of the overhead line, the first and the second traveling waves are used to calculate the fault location as:

$$x = L_L - \frac{v^{\text{line}} \cdot \blacktriangle t}{2} \tag{23}$$

where Δt [s] is the time delay between the fi rst and the second peak of scale-2 aerial mode voltage WTC2 s at bus S.

The next section presents the simulation results on a test system.

IV. SIMULATION RESULTS

The performance of the proposed fault location method is tested on a 230-kV, 60-Hz transmission line. Line lengths are assumed to be L_L=100 mi and L_C=20 mi. Transient simula-tions are carried out using ATP. Overhead line and underground cable are modeled as frequency-dependent using the data pro-vided in [31] and [32], respectively. The overhead line tower structure and underground cable layout are shown in Fig. 6. In this paper, the results for transposed lines are provided; how-ever the proposed method is also tested on untransposed lines with satisfactory results which are not provided due to space limitations. The sampling time interval of voltage measurement is 5 μs (sampling frequency, f_s=200 kHz). The aerial mode traveling wave velocities are calculated using ATP software at 37.5 kHz, which corresponds to the middle value in scale-2 (25 kHz–50 kHz). The velocities are 1.85×10^5 mi/s in overhead line and 0.98×10^5 mi/s in cable. MATLAB Wavelet Toolbox and SVM Toolbox [33] are used to implement the proposed method. Gaussian noise is introduced to the measured transient voltages and currents to account for measurement noise. The noise is assumed to have zero mean and standard deviation equal to 1% of the sampled voltage or current signal.

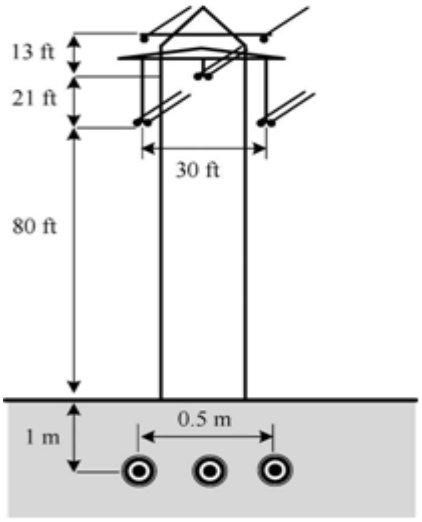

Fig. 6. Overhead line tower structure and underground cable layout.

Different fault scenarios under various system conditions(δ-loading ,FIA,R_f and location of the fault)are simulated to evaluate the performance of the proposed method. The simulations are carried out for the following cases:

1) δ=10◦ and 30 ◦
2) FIA=10◦,45◦,80◦ and 120 ◦
3) Rf=0.1Ω, 100 Ω
4) L_f=10% 20% 30% ...90% of the line and cable

A total of 2448 different cases that include all the conditions listed above are simulated. The feature extraction steps given in Section III.A are performed on all obtained simulation re-sults. The obtained input features and their corresponding outputs(i.e.,+1 for the faults in the line and -1 for the faults in the cable) in the first loading level ($\delta=10^0$) are used to train the SVM faulty –section/half identifiers.

The trained SVMs are then tested using the data set corre-sponding to all fault conditions at the second loading level. Other fault scenarios with different fault conditions (R_f and FIA) corresponding to the intermediate fault locations in the training set (e.g., fault occurring at δ=20◦,R=1.5Ω,L=35.5%) are also tested. The faulty-section identification accu-racy is calculated by using:

$$\eta = \frac{\#\text{ of accurately identified faulty sections}}{\#\text{ of test cases}} 100$$

The accuracies for SVM faulty-section/half identification with three different kernel functions are provided in Table I. Note that the Gaussian RBF has better accuracy than the other kernel functions as mentioned in Section II. The kernel function parameter (γ) is tuned to achieve sufficient accuracy. The iden-tification accuracy deteriorates during extreme cases when a high- resistance fault (i.e., 50Ω≤Rf≤100Ω) occurs at small fault inception angles (i.e., ≤5◦). This combination produces smaller wavelet coeffi cients leading to low signal energies which makes it difficult for SVMs to identify the faulty-section.

First scenario assumes that a phase a-to-ground fault occurs in overhead line at 87 miles from bus S. The fault conditions are assumed as follows: δ=20◦,FIA=35◦,Rf=0.5Ω. The output of faulty-section identifier SVM1 is +1 identifying

TABLE I
SVM FAULTY-SECTION/HALF IDENTIFICATION ACCURACY WITH DIFFERENT KERNEL FUNCTIONS

		η (%)
SVM_1	Gaussian RBF	98.8
	Polynomial	96.7
	Linear	82.9
SVM_2	Gaussian RBF	98.2
	Polynomial	94.2
	Linear	81.6
SVM_3	Gaussian RBF	95.6
	Polynomial	92.3
	Linear	80.8

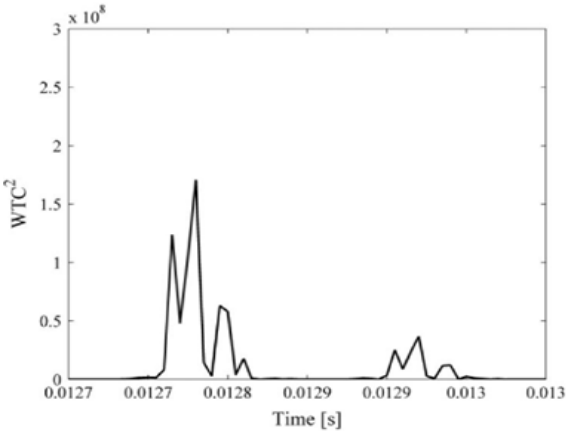

Fig. 7. Voltage WTC_2 s in aerial mode in scale-2 for a single-phase-to-ground fault in overhead line at 87 miles from bus S.

the faulty-section as the overhead line. SVM_2 for faulty- half identification in the line gives the output as –1 implying that the aerial mode (mode 1) voltage WTC_2 s at scale-2, shown in Fig. 7 is used for fault location. The time difference between the first and the second travelling waves peaks in WTC_2 s, Δt is observed as 140 μs. The fault location is then calculated by using (23):

$$x = 100 - \frac{14 \times 10^{-5} \times 1.85 \times 10^5}{2} = 87.05 \text{ mi}$$

Second scenario assumes that a b-to-ground fault occurs in underground cable at 103 miles from bus s(ie, 3 miles from J-point)with the conditions as $\delta=15^0$,R_f =10Ω and FIA=275^0 identification is performed using svm1 resulting in -1 which implies an underground cable fault. The faulty-half of the cable is then identified by using svm3.the svm3 gives the output as +1 impling that the fault is in the second half .Voltage WTC^2 in aerial mode at scale-2 at bus s is shown in figure 8.Δt is observed as 60 μs.The fault location is then calculated using (20).

$$x = 100 + \frac{6 \times 10^{-5} \times 0.98 \times 10^5}{2} = 102.94 \text{ mi}$$

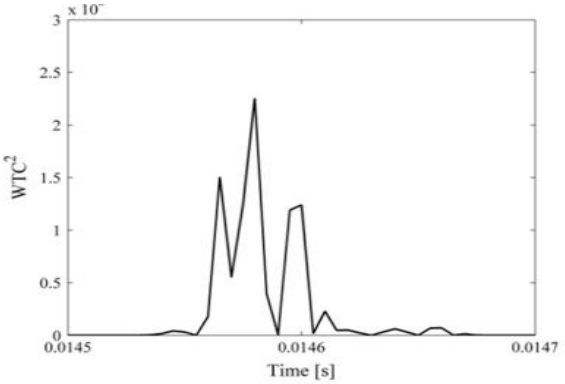

Fig. 8. Voltage WTC_2 s in aerial mode in scale-2 for a single-phase-to-ground fault in underground cable at 103 miles from bus S.

TABLE II
Fault Location Error For Different Case

Fault Section	Actual fault distance, AFD (mi)	Calculated fault distance, CFD (mi)	Error, e (%)
Line	5	5.55	0.55
	17	16.65	0.45
	23	23.12	0.12
	46	46.25	0.75
	84	83.35	0.65
	93	92.60	0.40
Cable	103	102.94	0.30
	105	104.41	2.95
	109	109.31	1.55
	115	115.10	0.50
	117	116.60	2.00
	118	118.04	0.20

As the common practice, the absolute error is calculated as a percentage of the total section length in order to evaluate the effectiveness of the proposed fault location method [24].

$$\text{Error} = \frac{\text{AFD} - \text{CFD}}{\text{Total Section Length}} 100 \quad (25)$$

where AFD is the actual fault distance and CFD is the calculated fault distance. Different cases of phase a- to-ground faults with 0.5 Ω fault resistance are considered. The results are presented in Table II. The calculated fault locations show good correlation with the actual fault locations. The fault locations in the under-ground cable are calculated with respect to bus S.

A. The Effect of Fault Inception Angle

The severity of the fault initiated transients is affected by dif-ferent fault inception angles; however, the use of normalized wavelet energies, E_N and E_N as input to the SVMs in the proposed method reduces these impacts. The results for four dif-ferent locations with respect to the changes in FIA are shown

TABLE III
FAULTY LINE IDENTIFICATION AND FAULT LOCATION FOR DIFFERENT FIA

Fault	*FIA* (°)	SVM_1	SVM_2	SVM_3	CFD (mi)	*e* (%)
AG at 35th mi of line, δ= 20°, R_f=0.5 Ω	7	1	1	n/a	35.15	0.15
	30	1	1	n/a		
	150	1	1	n/a		
	330	1	1	n/a		
BC at 67th mi of line, δ = 25°	45	1	-1	n/a	66.61	0.39
	170	1	-1	n/a		
	350	1	-1	n/a		
	352	1	-1	n/a		
CG at 7th mi of cable, δ = 20°, R_f=1.5 Ω	55	-1	n/a	1	6.60	2.00
	110	-1	n/a	1		
	300	-1	n/a	1		
	354	-1	n/a	1		
AG at 13rd mi of cable, δ = 20°, R_f=0.5 Ω	6	-1	n/a	-1	13.14	0.70
	25	-1	n/a	-1		
	100	-1	n/a	-1		
	340	-1	n/a	-1		

TABLE IV
FAULTY LINE IDENTIFICATION AND FAULT LOCATION FOR DIFFERENT

Fault	R_f (Ω)	SVM_1	SVM_2	SVM_3	CFD (mi)	*e* (%)
AG at 35th mi of line, δ= 20°	0.1	1	1	n/a	35.15	0.15
	2	1	1	n/a		
	70	1	1	n/a		
BC at 74th mi of line, δ = 25°	0.5	1	1	n/a	74.10	0.90
	1.5	1	-1	n/a		
	10	1	-1	n/a		
CG at 7th mi of cable, δ = 20°	0.01	-1	n/a	1	6.86	0.70
	5	-1	n/a	1		
	15	-1	n/a	1		
BG at 15th mi of cable, δ = 20°	1	-1	n/a	-1	14.60	2.00
	10	-1	n/a	-1		
	20	-1	n/a	-1		

in Table III. The results show that the faulty - section/half iden-tification methods give reasonably accurate results for a wide range of fault inception angles varying between 6◦ and 354◦ . The method has satisfactory performance for locating the faults occurring under different fault inception angles as demonstrated in Table III. Our investigations show that the misclassification zone around the middle point of the line or cable is 2 miles for extreme cases such as high-resistance (i.e., $R \geq 50\Omega$) faults or faults occurring at small fault inception angles (i.e., $FIA \leq 5^\circ$). The misclassification zone around the joint point is 3 miles for such cases.

B. The Effect of Fault Resistance

The performance of the proposed method is evaluated for a wide range of fault resistances. As in the case of small fault inception angles, high impedance faults (HIFs) affects the severity of the traveling waves, resulting in smaller signal energies. As mentioned in the previous subsection the use of E_N and E_N for faulty line/section identification, reduces the impacts of high-impedances faults. The performance of the method is tested for fault resistances varying from 0.1 to 70 Ω. The faulty-section/half identi fication results for various fault resistances are demonstrated in Table IV for different fault locations. The calculated fault distances and the corresponding errors do not change with fault resistance.

TABLE V
FAULTY LINE IDENTIFICATION AND FAULT LOCATION FOR DIFFERENT FAULT TYPE

Fault	Type	SVM_1	SVM_2	SVM_3	CFD (mi)	*e* (%)
8th mi of line, δ= 20°, R_f=0.5 Ω, *FIA*=15°	*AG*	1	1	n/a	7.6	0.40
	BCG	1	1	n/a		
	AC	1	1	n/a		
	ABCG	1	1	n/a		
18th mi of cable, δ= 25°, R_f=1 Ω, *FIA*=160°	*CG*	-1	n/a	-1	18.04	0.20
	ABG	-1	n/a	-1		
	BC	-1	n/a	-1		
	ABCG	-1	n/a	-1		

C. The Effect of Fault Type

The effects of fault type on the proposed method for faulty line and faulty-half identification procedures as well as on fault location are evaluated in this section. The fault location results for two different locations in the overhead line and underground cable with respect to the fault type are shown in Table V. Al-though different fault types affect the severity of the fault initi-ated traveling waves, the proposed method uses the normalized wavelet energies, E_N and E_N as the input to the SVMs. As the results show, the faulty-section/half identification methods give accurate results for four different fault types. Even though the arrival times of the traveling waves can vary slightly for dif-ferent types of faults at a specific location, the time delay be-tween consecutive traveling waves remains unchanged. As the time delay between the traveling waves is used to determine the fault location, the method gives satisfactory accuracy for lo-cating the faults occurring under different types as demonstrated in Table V.

D. The Effect of Non-Linear High Impedance Fault

The performance of the proposed method is evaluated for a non-linear high impedance fault (NLHIF) . The model of a dy-namic time-varying resistance is provided below [34]:

$$R_{arc} = \frac{1}{g} \tag{26}$$

$$\frac{dg}{dt} = \frac{1}{\tau}(G \quad g) \tag{27}$$

$$G = \frac{|i_{arc}|}{V_{st}} \tag{28}$$

where $R_{arc}[\Omega]$ is the arc resistance which varies with time, g is the time varying arc conductance, i [kA] is the arc current, G is the stationary arc conductance, V_{st} [kV] is the stationary arc voltage and τ is the arc time constant. The stationary arc voltage is estimated as:

$$v_{st} = (u_0 + r.|i_{arc}|)l \tag{29}$$

where u_0[V/cm] is the constant voltage parameter per arc length,r[mΩ/cm] is the resistive component per arc length and l [cm] is the arc length.The following parameters are used to simulate the fault [34]; u_0=9.6, r=1.6 ,l=350 and $\tau = 1ms$

A single- phase - to-ground NLHIF is assumed to be located at 66 miles away from bus S on the overhead line. The fault conditions are assumed as follows:δ=15^0 and FIA=310^0.

The method first identifies the faulty-section according to the output of SVM1 which is +1 . The SVM2 for half side detection in the overhead line gives the output as −1 . Thus the faulty-half is determined in the second half of the line. Voltage WTC2 s at bus S in aerial mode at scale- 2 are finally observed to detect the time delay between the first two peaks, which is 360 μs. The fault location is calculated by using (23):

$$x = 100 - \frac{36 \times 10^{-5} \times 1.85 \times 10^{5}}{2} = 66.70 \text{ mi}$$

Similar to the cases of small fault inception angles and high-resistance faults, a NLHIF also affects the magnitude of the trav-eling waves. The arrival times of the traveling waves are delayed due to the impact of non-linear impedance on reflection and re-fraction coefficients. However, the time difference between the first and the second traveling wave arrivals remains unaffected. The delay for the simulated fault is observed to be in the order of 300 μs when compared with a resistive fault.

E. The Effect of Non-Ideal Fault

The performance of the proposed fault location method is evaluated for a non-ideal short-circuit fault. The 0.5 Ω resis-tance is connected through a 2 Ω inductance to the ground. A b-to -ground fault is located at 26 miles in the overhead line. The faulty-section identification is first performed using SVM1 which gives output as +1 . The SVM2 for half side identifi er in the overhead line then gives the output −1 . Thus the fault sec-tion is identified in the first half of the line. The aerial mode voltage WTC2 s at bus S at scale-2 are used and Δt is observed as 290 μs. Thus, the fault location is calculated using (22):

$$x = \frac{29 \times 10^{-5} \times 1.85 \times 10^{5}}{2} = 26.83 \text{ mi}$$

Even though the magnitudes of the traveling waves decrease as in the case of high- impedance faults and it also delays the arrival of the traveling waves for 20 μs, the time difference be-tween the first two arriving waves remain unchanged. The pro-posed method gives satisfactory results in presence of non-ideal faults.

F. Discussions

1) Faulty-Half Identification: In this section, the perfor-mance of the proposed method for faulty-half identification is compared with that of an existing method. The time delay between the first traveling wave arrival in the ground and aerial mode WTC2 s, Δt_0 are used for faulty-half identifica-tion in single-ended wavelet-based methods. In these methods, faulty-half is identified by comparing Δt_0 with a pre-calculated time-delay for a fault located in the middle, Δt_m . For illustrative purposes, a phase b-to-ground fault is assumed to have occurred in the underground cable located at 5 miles from the joint (i.e., 105 miles from bus S). Fig. 9 shows the voltage WTC2 s at bus S in aerial and ground mode at scale-2. The time delay for a fault in the middle of the underground cable (i.e., 10 mi) obtained using ATP simulation is Δt_m is 50μs this example the observedΔt_0 is 40μs identifying the faulty-half accurately;however,very high precision isneededtocompare. Δt_m and Δt_0 It is also difficult to accurately calculate Δt_0 as fig 9 demonstrates theproximity of the instants of initial peaks.

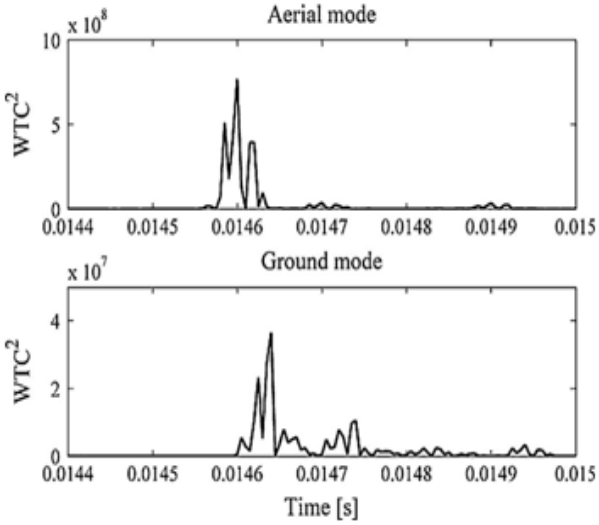

Fig. 9. Voltage WTC2 s at bus S in aerial and ground mode in scale-2 for a phase-b-ground fault at 105 miles away from bus S in underground cable.

The proposed method in this paper uses SVMs for faulty-half/section identification using the normalized wavelet ener-gies,E_{Nvk} and normalized transient current energies,E_{Nik} as input .the SVM_1output for faulty section identification gives -1 and the half-identifier svm2 for the cable is utilized to determine the faulty -half. The faulty-half is identifi ed as first half of the cable since the output of the SVM2 is +1 . The proposed method overcomes the precision problem pertinent to existing single-ended traveling wave methods using wavelet transform and Bewley diagram.

2) Cable Aging: The traveling wave velocity in cables decreases with aging due to the increase in cable inductance (L) [35]. The accuracy of single-

ended traveling wave- based fault location degrades as the electromagnetic traveling wave velocity in the cable changes during the years.

As an example, a phase a-to-ground fault is simulated in the aged underground cable located at 13 miles from the joint (i.e., 113 miles from bus S). The aged underground is simulated by increasing the relative permeability μ_r of each phase from 1 to 1.5.The fault conditions are $\delta=25^0$,R_f =1Ω and FIA=70^0. The observed Δt in the voltage WTC^2 at the bus s is 180 μs.

The traveling wave velocity calculated using ATP software at 37.5 kHz in the aged underground cable is 0.8×10^5 mi/s.

However, the fault location calculated by using the traveling Wave velocity in the original cable (i.e.,0.98*10^5 mi/s) is:

$$x = 100 + 20 - \frac{18 \times 10^{-6} \times 0.98 \times 10^5}{2} = 111.18 \text{ mi}$$

Note that the fault location error is 9.1%. As expected; the change in inductance due to aging affects the traveling wave-velocity, subsequently deteriorating the performance of the al-gorithm. This shortcoming can be addressed by introducing a correction factor, which translates the change in cable param-eters to a change in velocity. Correction factor can be deter-mined by carrying out site tests in certain time intervals or by employing a parameter estimation tool.

4.3 Single Line To Ground Fault

The circuit for simulating AC line fault for a given transmission line is shown in Fig. 10. If the circuit breaker is said to open then say switching times are given for 0.6 to 0.65 sec, then it implies that the circuit breaker closes at 0.6 sec and opens at 0.65 sec. So a fault period lies between 0.6 to 0.65 sec is observed on AC line. The fault voltage waves and current waves of an AC line fault are obtained in data acquisition box which was shown in Fig. 5.3&5.4. The reverse voltage travelling wave for the fault line is calculated using

$$V_r = [V_{ac} - Z_c * i_{ac}]/2$$

Where, V_r = reverse voltage travelling wave.

V_{ac} = voltage obtained during normal operation

I_{ac} = current obtained during normal operation

Z_c = surge impedance of the transmission line.

Reverse voltage travelling wave appears in the line only when, $Z_c > Z_t$ or $Z_c < Z$ where Z_c is the characteristic impedance of the transmission line where Z_t is the terminating impedance of the transmission line.

Line to ground fault on phase A

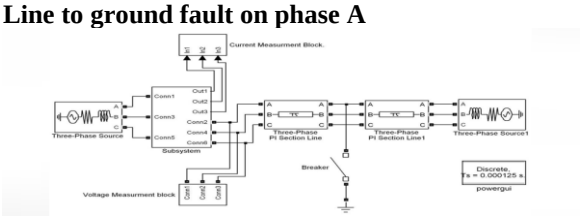

Fig.10 voltage signal during ac single line to ground fault

The fault occurs at a distance of 200km from the three phase source. The fault occurs from 0.6 seconds to 0.65 seconds for a period of 0.05 seconds. In the simulation diagram the block parameters and the switching times of the breaker are adjusted to be between 0.6 to 0.65 seconds. The wavelet modulus maxima which are obtained for faulted signal in case of a single line to ground fault are shown in Figures.

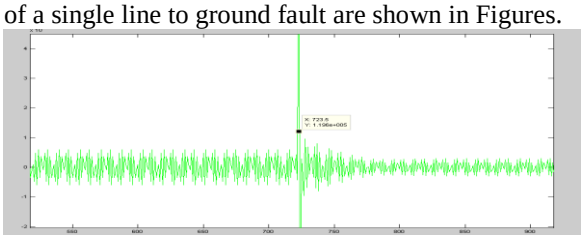

Fig. 11Wavelet modulus maxima signal for line to ground fault

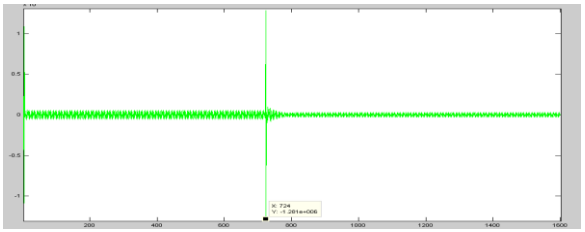

Fig.12 Wavelet modulus maxima signal for line to ground fault

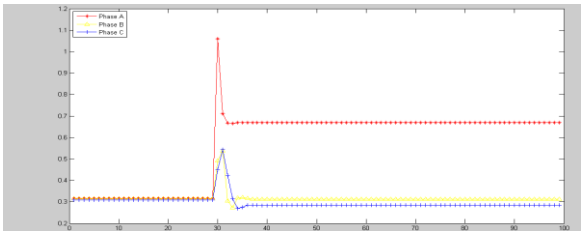

Fig.13 fault signal which occurred in line A

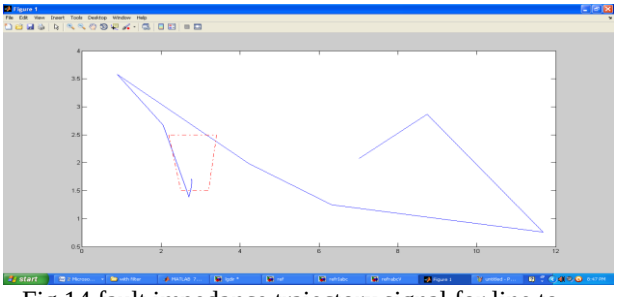

Fig.14 fault impedance trajectory signal for line to ground fault

Fault Calculations:

The value of the positive polared sample is obtained as N1=723.5 .The value of the negative polared sample is obtained as N2=723 .The total number of samples is obtained as N=1600 By knowing the values of N1, N2 and N, the value of Δt can be compared by using the equation shown below

Δt=(N2-N1)/N

Where (N2-N1) is the difference between the oppositely polared samples and N is the total number of samples.Δt is time delay between first two oppositely polared samples.The value of Δt is compared and is obtained as

Δt= (723.5-723)/1600 s.

Δt=0.00031s.

The distance of the fault location is calculated by the following equation,

L= (V*Δt)

Where V is the speed of the travelling wave=299750 km/s. L is the distance at which single line to ground fault occurred.The fault distance is computed and is obtained as

L=299750*0.00031 km

L=93.36 km.

Thus by using wavelet modulus maxima the fault distance is calculated. The fault is occurred at a distance of 93.36 km.

V. CONCLUSION

This paper proposes a single-ended traveling wave-based fault location method for a hybrid transmission line: an overhead line combined with an underground cable. Modal transformation and DWT are applied to the transient voltages recorded at the sending-end of overhead line. The normalized voltage wavelet energies and the normalized current energies are used for SVM faulty-section/half identification. The SVM classifiers use smaller set of inputs and are independent of fault type. The location of the fault is calculated by using the aerial mode voltage wavelets. The transient simulations are carried out using ATP software and the method is tested on MATLAB by using Wavelet Toolbox and SVM Toolbox. The performance of the proposed method is tested for various fault scenarios including different fault resistances, fault inception angles, fault locations, loading levels, non-linear high-impedance and non-ideal faults with satisfactory results.

REFERENCES

[1] M. Kezunovic, "*Smart fault location for smart grid*," *IEEE Trans. Smart Grid*, vol. 2, no. 1, pp. 11–22, Mar. 2011.

[2] P. K. Dash, S. R. Samantaray, and G. Panda, "*Fault classification and section identification of an advanced series compensated transmission line using support vector machine*," *IEEE Trans. Power Del.*, vol. 22, no. 1, pp. 67–73, Jan. 2007.

[3] U. B. Parikh, B. Das, and R. P. Maheshwari, "*Combined wavelet-SVM technique for fault zone detection in a series compensated transmission line*," *IEEE Trans. Power Del.*, vol. 23, no. 4, pp. 1789–1794, Oct. 2008.

[4] A. A. Yusuffa, C. Fei, A. A. Jimoha, and J. L. Munda, "*Fault location in a series compensated transmission line based on wavelet packet de-composition and support vector regression*," *Elect. Power Syst. Res.*, vol. 81, no. 7, pp. 1258–1265, Apr. 2011.

[5] R. Salat and S. Osowski, "*Accurate fault location in the power trans-mission line using support vector machine approach*," *IEEE Trans. Power Syst.*, vol. 29, no. 2, pp. 979–986, May 2004.

[6] J. A. Jiang, C. L. Chuang, Y. C. Wang, C. H. Hung, J. Y. Wang, C.H Lee, and Y. T. Hsiao, "*Hybrid framework for fault detection, clas-sification, and location Part I: Concept, structure, and methodology," IEEE Trans. Power Del.*, vol. 26, no. 3, pp. 1988–1997, Jul. 2011.

H. J. A. Jiang, C. L. Chuang, Y. C. Wang, C. H. Hung, J. Y. Wang, C.H. Lee, and Y. T. Hsiao, "*Hybrid framework for fault detection, clas-sification, and location Part II: Implementation and test results," IEEE Trans. Power Del.*, vol. 26, no. 3, pp. 1999–2008, Jul. 2011.

[7] X. Yang, M. S. Choi, S. J. Lee, C. W. Ten, and S. I. Lim, "*Fault location for underground power cable using distributed parameter approach*," *IEEE Trans. Power Syst.*, vol. 23, no. 4, pp. 1809–1816, Nov. 2008.

[8] Z. Xu and T. S. Sidhu, "*Fault location method based on single-end measurements for underground cables*," *IEEE Trans. Power Del.*, vol. 26, no. 4, pp. 2845–2854, Oct. 2011.

[9] M. S. Mashikian, R. Bansal, and R. B. Northorp, "*Location and char-acterization of partial discharge sites in shielded power cables," IEEE Trans. Power Del.*, vol. 5, no. 2, pp. 833–839, Apr. 1990.

[10] H. E. Gallagher, D. R. Mize, and A. F. Dickerson, "*Fault location system for transmission-type cable," IEEE Trans. Power App. Syst.*, vol. PAS-101, no. 6, pp. 1700–1710, Jun. 1982.

[11] C. M. Wiggins, D. E. Thomas, T. M. Salas, F. S. Nickel, and H. W. Ng, "*A novel concept for URD cable fault location,"*

IEEE Trans. Power Del., vol. 9, no. 1, pp. 591–597, Jan. 1994.

[12] N. Inoue, T. T. Tsunekage, and S. Sakai, "*On-line fault location system for 66 kV underground cables with fast O/E and fast A/D technique*," *IEEE Trans. Power Del.*, vol. 9, no. 1, pp. 579–584, Jan. 1994.

[13] F. H. Magnago and A. Abur, "*Fault location using wavelets," IEEE Trans. Power Del.*, vol. 13, no. 4, pp. 1475–1480, Oct. 1998.

[14] W. Zhao, Y. H. Song, and W. R. Chen, "*Improved GPS traveling wave fault locator for power cables by using wavelet analysis*," *Electr. Power Energy Syst.*, vol. 23, no. 5, pp. 403–411, Jun. 2001.

[15] M. Gilany, D. K. Ibrahim, and E. S. T. Eldin, "*Traveling-wave-based fault-location scheme for multiend-aged underground cable system*," *IEEE Trans. Power Del.*, vol. 22, no. 1, pp. 82–89, Jan. 2007.

[19] J. Sadeh and H. Afradi, "*A new and accurate fault location algo-rithm for combined transmission lines using adaptive network-based fuzzy inference system*," *Elect. Power Syst. Res.*, vol. 79, no. 11, pp. 1538–1545, Nov. 2009.

[20] D. Spoor and J. G. Zhu, "*Improved single-ended traveling-wave fault-location algorithm based on experience with conventional substation transducers*," *IEEE Trans. Power Del.*, vol. 21, no. 3, pp. 1714–1720, Jul. 2006.

[21] M. J. Reddy and D. K. Mohanta, "*A wavelet-fuzzy combined approach for classification and location of transmission line faults*," *Int. J. Electr. Power Energy Syst.*, vol. 29, no. 9, pp. 669–678, Nov. 2007.

[22] D. Chanda, N. K. Kishore, and A. K. Sinha, "*A wavelet multiresolu-tion analysis for location of faults on transmission lines," Int. J. Electr. Power Energy Syst.*, vol. 25, no. 1, pp. 59–69, Jan. 2003.

[23] C. K. Jung, K. H. Kim, J. B. Lee, and B. Klöckl, "*Wavelet and neuro-fuzzy based fault location for combined transmission systems*," *Int. J. Electr. Power Energy Syst.*, vol. 29, no. 6, pp. 445–454, Jul. 2007.

[24] I. Niazy and J. Sadeh, "*A new single ended fault location algorithm for combined transmission line considering fault clearing transients without using line parameters*," *Int. J. Electr. Power Energy Syst.*, vol. 44, no. 1, pp. 616–623, Jan. 2013.

[25] C. K. Jung, J. B. Lee, X. H. Wang, and Y. H. Song, "*Wavelet based noise cancellation technique for fault location on underground power cables," Elect. Power Syst. Res.*, vol. 77, no. 10, pp. 1342–1369, Aug. 2007.

[26] W. Zhao, Y. H. Song, and W. R. Chen, "*Improved GPS traveling wave fault locator for power cables by using wavelet analysis*," *Int. J. Electr. Power Energy Syst.*, vol. 23, no. 5, pp. 403–411, Jun. 2001.

[27] P. S. Bhowmik, P. Purkait, and K. Bhattacharya, "*A novel wavelet transform aided neural network based transmission line fault analysis method*," *Int. J. Electr. Power Energy Syst.*, vol. 31, no. 5, pp. 213–219, Jun. 2009.